Preprints of the 21st IFAC World Congress (Virtual)
Berlin, Germany, July 12-17, 2020

Pose Estimation and Tracking Control of a Pneumatic Soft Robotic Hand

J. Gastinger * **D. Müller** * **A. Hildebrandt** ** **O. Sawodny** *

* *Institute for System Dynamics, DE-70569 Stuttgart*
** *Festo AG & Co.KG, Robotics System Design, DE-73734 Esslingen*

Abstract: The use of soft robotics offers opportunities which cannot be achieved with conventional rigid robots, including adaptive interactions with humans (Kim et al. (2013)). This article presents the state estimation and tracking control for a soft robotic hand with 12 degrees of freedom (DOF). In the work, we achieve orientation estimation of phalanges and palm using a Multiplicative Extended Kalman-Filter (MEKF) yielding an average mean absolute error of less than 3.5°. Additionally, we use the estimated orientations for a tracking control for the finger poses. Experiments show that the estimated control variable can follow a sine trajectory as well as small precise step trajectories with an estimated control error of less than 3° which we consider sufficient to precisely target objects or copy gestures in real-time.

Keywords: Tracking Control, Soft Robotics, Pneumatic Systems, Robotic Hands, State Estimation, State Observers, Extended Kalman Filters, Inertial Measurement Units

1. INTRODUCTION

Research in the field of soft robotics has increased vastly in the last decade. Laschi et al. (2016) identify soft robots as a gateway towards more advanced or more efficient robot abilities that were not possible before with rigid robots. They name numerous benefits for the compliance of soft robots, e.g. their conformance to surfaces or objects, physical robustness and human safe operation at potentially low cost. The soft robot used for this article has been inspired by one of nature's most elaborate tools: the human hand. The Festo Bionic Learning Network recently introduced the BionicSoftHand, a pneumatically actuated hand with 12 DOF. This soft robotic hand with mounted sensor units is pictured in Figure 1. The BionicSoftHand was built with the goal of mimicking the human hand's grasping abilities. Potential applications are human robot interaction or remote control manufacturing using gesture imitation. This work focuses on tracking control to obtain precise finger movement and disturbance compensation. State reconstruction requires a state estimation algorithm, in this case, using Inertial Measurement Units (IMUs) and magnetometers.

1.1 State of the art

State Estimation using IMUs and Magnetometers The state estimation presented in this work bases on the work of Kok et al. (2017). Where Kok et al. (2017) describe the algorithm and probabilistic models for state estimation using inertial sensors and magnetometers, they do not apply state estimation for multiple sensor units at one timestep, or even finger poses, and thus their work differs from our work.

In the following, we show work on state estimation for fingers using IMUs and magnetometers which is mostly

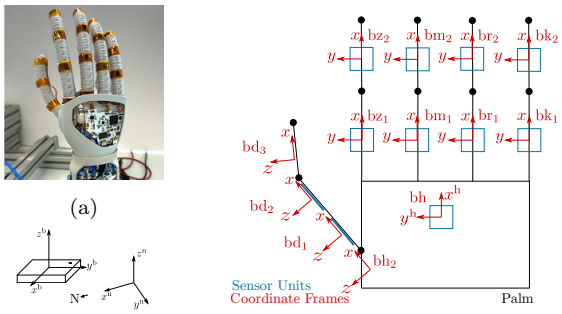

Fig. 1. (a) Upper part of the BionicSoftHand with sensor units on fingers and palm, (b) placement of the body frame on the sensor unit and the stationary navigation frame, (c) body frames and sensor units on the hand.

located in the field of medicine and biology, with applications in motion analysis of human hands or gesture recognition. A big part of solutions are wearables as described in Hammond et al. (2014). Due to its low computational complexity, the Madgwick algorithm by Madgwick et al. (2011) is implemented by Lin et al. (2017), Lin et al. (2018) and Valtin et al. (2018) for finger pose estimation with IMUs and magnetometers. An Extended Kalman Filter (EKF) using IMU and magnetometer data for human finger pose estimation is implemented in Kortier et al. (2014) and Hsiao et al. (2015). Kortier et al. (2014) extend a multiplicative EKF (MEKF) by a plausibility check of sensor data and by the inclusion of kinematic constraints caused by the morphology of the hand as artificial measurements. Kaczmarek and Tomczyński (2016) estimate the pose of a robot finger using a model which accounts kinematic constraints of joints. In experiments they compare estimates of Madgwick algorithm to EKF estimates. They state that EKF estimates resulted in lower errors, especially for movements faster than 30°/s.

Control of Soft Robots In general the control of soft robots and especially soft continuum manipulators is still an open topic as stated in Rus and Tolley (2015) who give an overview of design, fabrication, modeling and control of different soft robot structures. According to George Thuruthel et al. (2018) model-based static controllers are currently the most widely used strategy for control of continuum/soft robots, where the majority of works rely on the constant curvature (CC) approximation. They also describe that for multi-section manipulators, each constant curvature section can be stitched together to provide the piecewise CC (PCC) model, as used e.g. in Marchese and Rus (2016) for the control of a soft spatial fluidic elastomer manipulator. Falkenhahn (2017) presents model-based tracking control of actor coordinates for continuum manipulators. A numerically exact approach for soft robotic modeling and control bases on finite element analysis (FEM) as presented by Coevoet et al. (2019), and Katzschmann et al. (2019) who design a dynamically closed-loop controlled soft robotic arm using model order reduction. Della Santina et al. (2018) describe a dynamic formulation of a soft robotic structure similar to fingers under the assumption that the piecewise constant-curvature approach is applicable. Deimel and Brock (2016) present an underactuated compliant robot hand, where fingers are realized as pneumatic continuum-actuators being modeled using a CC approach. They implement feed forward control for finger poses but do not measurefinger orientations. For more information on recent control strategies for soft robotic manipulators, we refer to the survey of George Thuruthel et al. (2018) who present work on model-based, as well as model-free, and hybrid controllers.

1.2 Contribution and Road Map

The fingers in this work do not have firm joints but a soft structure. We do renounce a classical kinetic derivation of model equations. Our work differs from presented work on control of soft robots in that we do not derive model equations, and do not use any of the presented concepts. We show in experiments, that our straightforward control approach leads to results which we consider sufficient to precisely target objects and copy gestures in real-time. The presented work on state estimation differs in the application for human hands: with one exception, all introduced literature uses data gloves or systems mounted directly on the hands, often human bone structure is directly used for computation. Further, estimated poses from stated work are not used for control but e.g. for motion analysis.

The contribution of this work is the implementation and development of a tracking control including state estimation for a novel humanoid soft robotic hand. To the best knowledge of the authors, this has not been done before. Previous approaches either exclusively focused on state estimation or implemented feed forward control.

We present the problem formulation, hardware and theoretical background in Section 2. Section 3 deals with our solution approach, including probabilistic models, state estimation and tracking control. In Section 4 we show and discuss experimental results, and Section 5 gives a conclusion.

2. PROBLEM FORMULATION

2.1 Hardware with focus on sensor units

The BionicSoftHand, introduced by Festo AG & Co. KG (2019), is a pneumatically actuated hand with 12 DOF. Its fingers consist of elastomer bellows, which are enclosed in a special 3D knitted textile cover.

Increasing air pressure inside the elastomer bellows leads to finger bending, decreasing pressure leads to a stretched position. Each finger features two DOF, realized by two air chambers in the bellows. Thumb and index finger each feature a third DOF, implemented as swivel module, which allows them to perform lateral movements. As the fingers' motions strongly remind of human phalanges' movements, we use the term lower and upper phalanx to describe the fingers' air chambers. The pressure control is performed by a digitally controlled valve terminal.

The BionicSoftHand is equipped with a total of 11 Bosch BNO055 sensor units. Each of them consists of an IMU with accelerometer and gyroscope and a magnetometer. One sensor unit is placed on the palm, the other units are placed on the phalanges. The Bosch BNO055 sensor units integrate a proprietary sensor fusion algorithm for orientation estimation. We compare the results of our approach to the Bosch BNO055 estimates. Measurements at time step t consist for each sensor unit on phalanx s of measurements from accelerometer $\boldsymbol{y}_{\mathrm{a},t,s}$, magnetometer $\boldsymbol{y}_{\mathrm{m},t,s}$ and gyroscope $\boldsymbol{y}_{\omega,t,s}$.

2.2 Theoretical Foundation

For the description of coordinate frames, we use the convention presented in (Kok et al., 2017, p. 9 f.) and define a body coordinate frame b as well as a stationary navigation coordinate frame n. A superscript describes which frame a vector is represented. Vectors can be rotated between coordinate frames using quaternions or rotation matrices, which we indicate by a double superscript, e.g. $\boldsymbol{v}^{\mathrm{n}} = \boldsymbol{R}^{\mathrm{nb}}\boldsymbol{v}^{\mathrm{b}}$, (Kok et al., 2017, p. 10). The b-frame is placed on the moving sensor unit, where we define one b-frame for each sensor unit as illustrated in Figure 1(b). We define the b-frames used for orientation estimation of the fingers as in Figure 1(c) and describe sensor measurements in the respective b-frame. The n-frame is a local geographic coordinate frame, stationary and defined relative to the earth, with the x-axis pointing north. For orientation estimation, the orientation of each b-frame with respect to the n-frame $\boldsymbol{R}^{\mathrm{nb}}$ is computed.

Orientation in this work is parametrized by rotation matrices $\boldsymbol{R}$ or quaternions $\boldsymbol{q}$. The used notation follows the convention introduced in Kok et al. (2017). We employ a method described in (Kok et al., 2017, p. 21) to represent orientation for estimation algorithms. An orientation $\boldsymbol{q}_t^{\mathrm{nb}}$ is described as linearization point (unit quaternion $\tilde{\boldsymbol{q}}_t^{\mathrm{nb}}$ or rotation matrix $\tilde{\boldsymbol{R}}_t^{\mathrm{nb}}$) and orientation deviation (rotation vector $\boldsymbol{\eta}_t$), where the subscript t describes the time step. Thus with quaternion multiplication $\odot$ and the quaternion representation $\bar{\boldsymbol{\eta}}$ of $\boldsymbol{\eta}$ we have

$$\boldsymbol{q}_t^{\mathrm{nb}} = \exp\left(\frac{\bar{\boldsymbol{\eta}}_t^{\mathrm{n}}}{2}\right) \odot \tilde{\boldsymbol{q}}_t^{\mathrm{nb}} = \exp_{\mathrm{q}}\left(\frac{\boldsymbol{\eta}_t^{\mathrm{n}}}{2}\right) \odot \tilde{\boldsymbol{q}}_t^{\mathrm{nb}}, \qquad (1)$$

where

$$\exp(\bar{\boldsymbol{\eta}}) = \begin{pmatrix} \cos\|\boldsymbol{\eta}\|_2 \\ \frac{\boldsymbol{\eta}}{\|\boldsymbol{\eta}\|_2}\sin\|\boldsymbol{\eta}\|_2 \end{pmatrix}, \tag{2}$$

and where we use the mapping

$$\boldsymbol{q} = \exp_{\mathrm{q}}(\boldsymbol{\eta}), \quad \exp_{\mathrm{q}} : \mathbb{R}^3 \to \left\{\boldsymbol{q} \in \mathbb{R}^4 \colon \|\boldsymbol{q}\|_2 = 1\right\}. \tag{3}$$

For the derivation of equation (1) we refer to (Kok et al., 2017, p. 19).

2.3 Problem Formulation

The goal of this work is the implementation of an estimation and tracking control for fingers of a pneumatically actuated robot hand with 12 DOF. Each DOF d is a rotation of one phalanx i around the z-axis for the third DOF on index finger and thumb or the y-axis for all other DOF of the reference coordinate frame. Elements $\boldsymbol{q}_{t,d}$ of the controlled variable $\boldsymbol{q}_t$ describe the rotation of phalanges with respect to palm for lower phalanges or with respect to adjacent phalanges for upper phalanges around the respective axis for each DOF d. The problem formulation in this work can be split into two problems:

Problem 1. (*State Estimation*). The estimated controlled variable $\hat{\boldsymbol{q}}_{t,d}$ should be determined from given measurements $\boldsymbol{y}_{\mathrm{a},t,s}, \boldsymbol{y}_{\mathrm{m},t,s}, \boldsymbol{y}_{\omega,t,s}$, so that ideally at each time step t for each sensor unit s and each DOF d we have $\hat{\boldsymbol{q}}_{t,d} = \boldsymbol{q}_{t,d}$.

Problem 2. (*Tracking Control*). Using the reconstructed state $\hat{\boldsymbol{q}}_{t,d}$, the controlled variable $\boldsymbol{q}_{t,d}$ should follow the given reference variable $\boldsymbol{w}_{t,d}$, so that ideally at each time step t for each DOF d we have $\boldsymbol{q}_{t,d} = \boldsymbol{w}_{t,d}$. Thus our goal is to minimize the control error $\boldsymbol{e}_{t,d}$, where $\boldsymbol{e}_{t,d} = \boldsymbol{w}_{t,d} - \boldsymbol{q}_{t,d}$.

3. SOLUTION APPROACH

3.1 Probabilistic Models

We show the state model used for orientation estimation for all sensor units $k = 1, ..., K$ on a single finger including palm $k = 1$. We assume that the sensors do not travel over significant distances compared to the size of the earth. Additionally, earth rotation and linear acceleration of the sensor units are assumed to be negligibly small. We assume that time steps t in which states are defined, are in accordance with the sensor's sampling times. Further, we assume that the magnetometer only measures the earth's magnetic field and that constant offsets in sensor measurements are eliminated during calibration. Then the state model is defined as

$$\boldsymbol{q}^{\mathrm{nb}}_{t+1,k} = \boldsymbol{q}^{\mathrm{nb}}_{t,k} \odot \exp_{\mathrm{q}}\left(\frac{T}{2}(\boldsymbol{y}_{\omega,t,k} - \boldsymbol{r}_{\omega,t})\right), \tag{4a}$$

$$\boldsymbol{y}_{\mathrm{a},t,k} = -\boldsymbol{R}^{\mathrm{bn}}_{t,k}\boldsymbol{g}^{\mathrm{n}} + \boldsymbol{r}_{\mathrm{a},t}, \tag{4b}$$

$$\boldsymbol{y}_{\mathrm{m},t,k} = \boldsymbol{R}^{\mathrm{bn}}_{t,k}\boldsymbol{m}^{\mathrm{n}} + \boldsymbol{r}_{\mathrm{m},t}, \tag{4c}$$

with gravitational acceleration vector $\boldsymbol{g} \approx [0, 0, 9.81]^{\mathrm{T}}$ and earth magnetic field $\boldsymbol{m}^{\mathrm{n}} = [\cos\delta, 0, \sin\delta]^{\mathrm{T}}$ where δ describes the dip angle. Equations (4b) to (4c) describe the measurement models with $\boldsymbol{y}_{\omega,t,k}, \boldsymbol{y}_{\mathrm{a},t,k}, \boldsymbol{y}_{\mathrm{m},t,k} \in \mathbb{R}^{3\times 1}$ and $\boldsymbol{r}_{\omega,t} \sim \mathcal{N}(\boldsymbol{0}, \boldsymbol{\Sigma}_{\omega})$, $\boldsymbol{r}_{\mathrm{a},t} \sim \mathcal{N}(\boldsymbol{0}, \boldsymbol{\Sigma}_{\mathrm{a}})$, $\boldsymbol{r}_{\mathrm{m},t} \sim \mathcal{N}(\boldsymbol{0}, \boldsymbol{\Sigma}_{\mathrm{m}})$. In this context $\boldsymbol{\Sigma}_{\omega} = \sigma^2_{\omega}\mathcal{I}_3$, $\boldsymbol{\Sigma}_{\mathrm{m}} = \sigma^2_{\mathrm{m}}\mathcal{I}_3$, $\boldsymbol{\Sigma}_{\mathrm{a}} = \sigma^2_{\mathrm{a}}\mathcal{I}_3$, represent measurement noise as well as model uncertainties, where $\mathcal{I}_3$ is the identity matrix. For the derivation of equations (4a), (4b), (4c) we refer to (Kok et al., 2017, p. 30 f.).

For initialization of $\boldsymbol{q}^{\mathrm{nb}}_{1,k}$ we implement the QUEST algorithm introduced in (Kok et al., 2017, p. 27 f.).

3.2 State estimation

For orientation estimation with given sensors, we implement a MEKF, a subgroup of the EKF. We parametrize orientation as orientation deviation from a linearization point. The linearization point $\tilde{\boldsymbol{q}}^{\mathrm{nb}}_t$ is defined as the last step estimate. Deviation from that linearization point $\boldsymbol{\eta}^{\mathrm{n}}_t$ constitutes the state vector in the MEKF. As the deviation from the linearization point is normally very small, it can be parametrized as rotation vector without loss of information as no singularities occur. Thus the state to estimate one sensor unit's orientation has 3 dimensions instead of 4 dimensions with quaternion representation, leading to less computational costs. We use the MEKF algorithm introduced in (Kok et al., 2017, p. 39 ff.).

State dynamics of $\boldsymbol{\eta}^{\mathrm{n}}$ are given with steps size T by

$$\boldsymbol{\eta}^{\mathrm{n}}_{t+1} = \boldsymbol{f}_t(\boldsymbol{\eta}^{\mathrm{n}}_t, \boldsymbol{y}_{\omega,t}, \boldsymbol{r}_{\omega,t}) = 2\log\left(\exp_{\mathrm{q}}(\frac{\boldsymbol{\eta}^{\mathrm{n}}_{\omega,t}}{2}) \odot \tilde{\boldsymbol{q}}^{\mathrm{nb}}_t \odot \exp_{\mathrm{q}}(\frac{T}{2}(\boldsymbol{y}_{\omega,t} - \boldsymbol{r}_{\omega,t})) \odot \tilde{\boldsymbol{q}}^{\mathrm{bn}}_{t+1}\right). \tag{5}$$

We describe the steps of the MEKF algorithm as follows. In the *Time Update* step, we use gyroscope measurements to update the linearization point and covariance matrix $\boldsymbol{P}$. During the *Measurement Update*, the state and covariance matrix are updated using accelerometer and magnetometer measurements. In the *Relinearization step*, we update the linearization point $\tilde{\boldsymbol{q}}^{\mathrm{nb}}_t$ and reset the state $\boldsymbol{\eta}^{\mathrm{n}}_t$.

Filter Design We implement one MEKF per finger. Thus, in total, for orientation estimation on the BionicSoftHand we use 5 MEKF. One MEKF estimates the orientation of palm h, lower f_1 and upper phalanx f_2 with respect to the n-frame for one finger f, $\hat{\boldsymbol{q}}^{\mathrm{nbh}}$, $\hat{\boldsymbol{q}}^{\mathrm{nbf}_1}$, $\hat{\boldsymbol{q}}^{\mathrm{nbf}_2}$.

Plausibility Check Measurement values are checked for plausibility before being used for state estimation, adapted from Kortier et al. (2014). For each sensor unit s we consider the following criteria:

(1) Calibration status of respective measurement
(2) Deviation of magnetometer measurements' norm at time step t from norm at time step $t = 1$
(3) Spikes in gyroscope measurements
(4) Presence of linear acceleration, judged by observation of angular velocity norm
(5) Deviation of accelerometer measurements' norm on one phalanx to norm on adjacent phalanx on same finger

The accepted measurements are appended to the measurement vector $\boldsymbol{y}_t$. In case no measurement is accepted in this step, the prediction is not corrected. For gyroscope measurements used in the prediction step applies the following: If the measurement on one phalanx is rejected, but the measurement on the adjacent phalanx accepted, we use this adjacent measurement for both sensors. If both

phalanges' measurements are rejected, we artificially set the values to $\boldsymbol{y}_{\omega,t,\mathrm{f}} = [0,0,0]^{\mathrm{T}}$.

3.3 Tracking Control

The control of the BionicSoftHand is realized in a cascade structure. This structure enables a detached design of the two components, the underlying pressure control and the overlying position tracking control. This work focuses on position tracking control, where positions of phalanges should follow given setpoint trajectories.

Setpoint Specification As setpoint for each DOF d at each time step t a target angle is specified. We transform angles to quaternions. Transformed setpoint values enter the control loop as reference variable $\boldsymbol{w}_t$.

System Characteristics The BionicSoftHand fingers have a soft structure and low mass. Fingers do not have strict joints. Movement is realized by modifying air pressure in the bellow structures. On the upper thumb phalanx, no sensor unit is mounted due to hardware reasons. Thus we cannot conclude on its orientation. This means that the state describing the rotation of the upper thumb phalanx is not observable. For this reason, no feedback control is possible for the position of the upper thumb phalanx. Instead, we use an empirically fitted pressure-angle-curve for feed forward control.

Design of Tracking Controller For tracking control we use a decentralized control concept. We assume that the DOF are decoupled. The plant consists of the underlying pressure control and of fingers equipped with sensor units. A disturbance $\boldsymbol{z}_t$ acts on the plant, thus the controlled variable $\boldsymbol{q}_t = [\boldsymbol{q}_{t,1}, \boldsymbol{q}_{t,2}, \ldots, \boldsymbol{q}_{t,12}]^T$ depends on the control signal $\boldsymbol{u}_t$ and the disturbance $\boldsymbol{z}_t$. As control signal $\boldsymbol{u}_t$, at each time step t a pressure vector $\boldsymbol{p}_t$ with in total 12 values is returned to the pressure controller, $\boldsymbol{u}_t = \boldsymbol{p}_t$. From the estimated controlled variable $\hat{\boldsymbol{q}}_t$ and the specified reference variable $\boldsymbol{w}_t$ the control error $\boldsymbol{e}_t$ can be computed at each time step.

We realize the tracking control as a 2-DOF control structure. Thus, the control signal $\boldsymbol{u}_t$ consists of a signal describing feed forward control $\boldsymbol{u}_{V,t}$ and a signal describing feedback control $\boldsymbol{u}_{R,t}$. Both parts are designed independently. The feed forward control is chosen to trace the controlled variable as fast as possible to the reference variable. The feed forward control improves performance by using the reference signals. For this, we use an angle-pressure-curve, that maps a pressure value to each angle value. We generate this angle-pressure-curve by fitting experimental values. We implement the feedback control as PID controller and determine values for P-, D- and I-parameters experimentally. The system's stability threshold can be determined experimentally. This is feasible, as it is possible to run the process at the stability threshold for a short time period. To guarantee the adherence to control variable restriction, we include a saturation of control signals. Additionally, we implement anti-windup, turning off the integral part when saturation is reached.

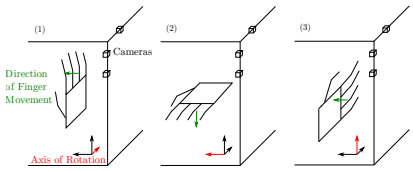

Fig. 2. Different placements of the BionicSoftHand.

4. RESULTS AND DISCUSSION

4.1 State estimation

To test the implemented EKF for orientation estimation of phalanges, we run three test rows with different setups. One run with a certain setup is denoted experiment. To survey estimation results, we use an optical reference system: three Point Grey cameras of type BFLY-PGE-13E4M-CS are mounted on a frame as illustrated in Figure 2. Infrared emitters are attached to sensor units on the BionicSoftHand. We compute the deviation of orientation estimates to orientations measured by infrared emitters. Furthermore, we compare the estimation deviations from the implemented EKF algorithm to the estimation deviations from the BNO055 internal orientation estimation algorithm. In the following, experiment results from the implemented EKF algorithm are denoted by EKF, results from the BNO055 estimation algorithm are denoted by BNO. We run all experiments with fully calibrated sensors. In this article, we exemplary examine the Rotation $\boldsymbol{R}^{\mathrm{bhbr}_1}$ of the lower ring finger phalanx r_1 w.r.t. palm h with coordinate frames br_1 and bh respectively.

In *Test Row 1* we test the EKF without extensions, i.e. no plausibility check to examine the basic functionality of the implemented EKF. We run tests of the algorithm in the three different placements of the BionicSoftHand illustrated in Figure 2. Experiment 1.1 is run in placement 1, experiment 1.2 in placement 2 and 1.3 in placement 3. We consider different placements, as the EKF should deliver reasonable results for all placements even though the accelerometer can not measure rotation around the axis pointing to the earth's center. Each experiment is run for 70 seconds. Additionally, we present estimation errors for a longer time period to monitor drift of estimates with time. Figure 3 shows the mean absolute error (MAE) of EKF and BNO estimate in degree over a time period of 70 (a) and 500 (b) seconds for hand placement 1. The periodic small spikes are caused by the algorithm of the reference system. Figure 4 shows the trajectories from EKF and BNO estimates as well as measurements from the reference system in quaternion representation corresponding to results from figure 3(a).

Graphs for experiments 1.2 and 1.3 do not considerably differ from the graph shown in Figure 3 and are thus omitted. Table 1 summarizes results for Test Row 1 in form of mean values of MAE per experiment for EKF and BNO. Note that in each experiment the mean MAE EKF are smaller than the mean MAE BNO.

In *Test Row 2* the focus lies on the implemented extension of plausibility check as well as the repeatability of experiment results. Experiments are conducted in hand placement 1 and repeated five times. As graphs do not dif-

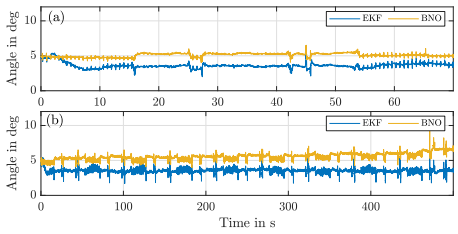

Fig. 3. Deviation (MAE) of EKF and BNO to reference measurements for two experiments.

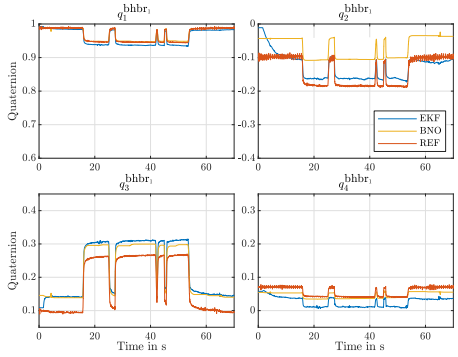

Fig. 4. Estimate of EKF, BNO and reference measurements (REF) for experiment 1.1 (70 s).

Table 1. Summary of results for Test Row 1, all 70 s.

Experiment	1.1	1.2	1.3	Mean
Mean MAE EKF [deg]	3.610	2.168	3.453	3.077
Mean MAE BNO [deg]	5.102	2.553	3.802	3.819

fer significantly from the graph shown in Figure 3, figures are omitted. Results for Test Row 2 are summarized with execution time in Table 2. Mean MAE for EKF for Test Row 2 is lower than mean MAE for the same placement of hand in Test Row 1 (experiment 1.1).

Table 2. Summary of results for Test Row 2.

Experiment	2.1	2.2	2.3	2.4	2.5	Mean
Time	70 s	70 s	70 s	70 s	500 s	
Mean MAE EKF [deg]	3.151	3.970	3.812	2.586	3.734	3.451
Mean MAE BNO [deg]	3.912	3.888	3.526	4.030	3.764	3.824

Discussion From Test Row 1 we conclude that the EKF version without extensions gives reasonable estimates for all hand placements. In Figure 3 (bottom) it can be observed that EKF estimates do not drift over time, contrary to BNO estimates. From experiment 1.1 we conclude, that the EKF can correct initially wrong estimates over time as the estimation error decreases in the first seconds. Test Row 2 shows a lower mean EKF MAE than Test Row 1 for the same hand placement. This indicates that the plausibility check improves orientation estimation. In summary, we conclude that the implemented EKF algorithm reaches lower errors for phalanges' orientation estimation than the BNO internal orientation estimation algorithm. The plausibility check extension reduces estimation errors. The mean MAE EKF is below 3.5°.

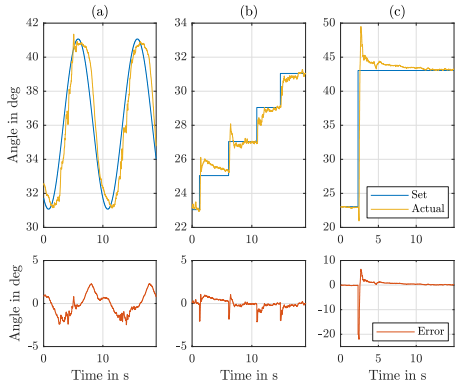

Fig. 5. Setpoint and estimated actual trajectories (top) and respective control error (bottom).

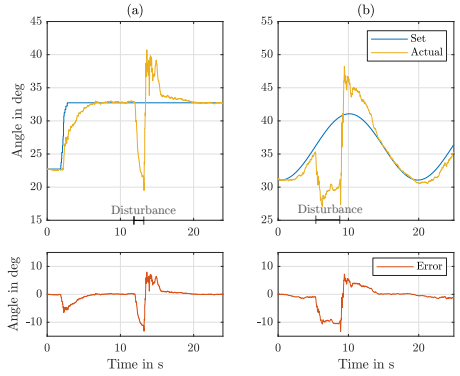

Fig. 6. Setpoint and estimated actual trajectories at external disturbance with (a) constant setpoint and (b) sine function as reference input. The disturbance period is marked on the respective x-axis.

4.2 Tracking Control

We show exemplary results of phalanx r_1 for representative setpoint trajectories and estimated actual trajectories and the control error in Figure 5. In Figure 5(a) and Figure 5(b) we show that the estimated control signal follows the setpoint variable for small, precise movements. In Figure 5(c) we define a step as setpoint trajectory. After overshoot, the control error approaches zero. In Figure 6 we illustrate the disturbance response in two examples. To cause disturbance, we manually moved and blocked the finger for a certain period. On the upper graphs in Figure 6, we plot the setpoint trajectory and estimated actual trajectory over time and mark the disturbance. In the bottom graphs, we show the control error. We observe that after an overshoot period this error approaches zero.

Discussion From results in Figure 5 we conclude that the command input response is sufficiently well for the application of the BionicSoftHand. The estimated control variable can follow a sine trajectory as well as small precise step trajectories with an estimated control error of less than 3°. From the results shown in Figure 6, we conclude that the 2-DOF controller reacts sufficiently well to disturbances. We note that this is not only caused by the implemented controller but also by the material stiffness of the fingers.

5. CONCLUSION AND FUTURE WORK

In this work, we realized a tracking control and position estimation for the position of fingers on a soft robotic hand with 12 DOF. The state estimation was implemented using one MEKF per finger. Additionally, we implemented a plausibility check for sensor measurements which rejects erroneous measurement values. The MEKF can estimate the phalanges' orientation with a mean absolute error less than 3.5° for different placements of the hand and for measurements over different time periods. We realized the tracking control using a 2-DOF structure and a decentralized control concept. As estimated actual control value we used the estimated orientation of the phalanges. For feed forward control, we experimentally fitted an angle-pressure-curve. We demonstrated the functionality of the tracking controller. The tracking control can be used to precisely target objects or to copy gestures in real-time.

5.1 Future Work

A possible task to build on this work is the combination of the implemented feedback position tracking control with a feedback force control using a hybrid control concept. In this context, the tactile force sensors, integrated in the BionicSoftHand could be used to detect contact force. At the occurrence of contact force, switching from position to force feedback control would be possible. This could help to not only guarantee the precise targeting of objects but also facilitate the gripping of objects. Because of the hand's soft structure, it is possible to grip sensitive objects, e.g. vegetables, of different shapes. In this case, the BionicSoftHand could be used in an industrial environment. When combining the BionicSoftHand with a collaborative robot arm, it might also be possible to use the BionicSoftHand in a collaborative work environment because of it's soft, compliant structure.

ACKNOWLEDGEMENTS

The authors gratefully acknowledge support of this work by the German Research Foundation (DFG) under grant SA 847/20-1. Further, we thank the Festo Bionic Learning Network for the opportunity to work on the BionicSoftHand and their support during our work.

REFERENCES

Coevoet, E., Escande, A., and Duriez, C. (2019). Soft robots locomotion and manipulation control using FEM simulation and quadratic programming. In *RoboSoft 2019 - IEEE International Conference on Soft Robotics*. Seoul, South Korea.

Deimel, R. and Brock, O. (2016). A novel type of compliant and underactuated robotic hand for dexterous grasping. *The International Journal of Robotics Research*, 35(1-3), 161–185.

Della Santina, C., Katzschmann, R.K., Biechi, A., and Rus, D. (2018). Dynamic control of soft robots interacting with the environment. In *2018 IEEE International Conference on Soft Robotics (RoboSoft)*, 46–53. IEEE.

Falkenhahn, V. (2017). *Modellierung und modellbasierte Regelung von Kontinuum-Manipulatoren*. Aachen: Shaker Verlag.

Festo AG & Co. KG (2019). Bionicsofthand. 73734 Esslingen Germany. URL `https://www.festo.com/group/de/cms/13508.htm`.

George Thuruthel, T., Ansari, Y., Falotico, E., and Laschi, C. (2018). Control strategies for soft robotic manipulators: A survey. *Soft robotics*, 5(2), 149–163.

Hammond, F.L., Menguc, Y., and Wood, R.J. (2014). Toward a modular soft sensor-embedded glove for human hand motion and tactile pressure measurement. In *2014 IEEE/RSJ International Conference on Intelligent Robots and Systems*. IEEE.

Hsiao, P.C., Yang, S.Y., Lin, B.S., Lee, I.J., and Chou, W. (2015). Data glove embedded with 9-axis IMU and force sensing sensors for evaluation of hand function. In *2015 37th Annual International Conference of the IEEE Engineering in Medicine and Biology Society (EMBC)*.

Kaczmarek, Piotrand Mańkowski, T. and Tomczyński, J. (2016). IMU-based kinematic chain pose estimation using extended kalman filter. In *Advances in Cooperative Robotics*, 331–338. World Scientific.

Katzschmann, R.K., Thieffry, M., Goury, O., Kruszewski, A., Guerra, T.M., Duriez, C., and Rus, D. (2019). Dynamically closed-loop controlled soft robotic arm using a reduced order finite element model with state observer. In *2019 2nd IEEE International Conference on Soft Robotics (RoboSoft)*, 717–724. IEEE.

Kim, S., Laschi, C., and Trimmer, B. (2013). Soft robotics: a bioinspired evolution in robotics. *Trends in Biotechnology*, 31(5), 287–294.

Kok, M., Hol, J., and Schoen, T. (2017). Using inertial sensors for position and orientation estimation. *Foundations and Trends in Signal Processing*, 11(1-2).

Kortier, H.G., Sluiter, V.I., Roetenberg, D., and Veltink, P.H. (2014). Assessment of hand kinematics using inertial and magnetic sensors. *Journal of NeuroEngineering and Rehabilitation*, 11(1).

Laschi, C., Mazzolai, B., and Cianchetti, M. (2016). Soft robotics: Technologies and systems pushing the boundaries of robot abilities. *Sci. Robot*, 1(1), eaah3690.

Lin, B.S., Hsiao, P.C., Yang, S.Y., Su, C.S., and Lee, I.J. (2017). Data glove system embedded with inertial measurement units for hand function evaluation in stroke patients. *IEEE Transactions on Neural Systems and Rehabilitation Engineering*, 25(11), 2204–2213.

Lin, B.S., Lee, I.J., Yang, S.Y., Lo, Y.C., Lee, J., and Chen, J.L. (2018). Design of an inertial-sensor-based data glove for hand function evaluation. *Sensors*, 18(5), 1545.

Madgwick, S.O.H., Harrison, A.J.L., and Vaidyanathan, R. (2011). Estimation of IMU and MARG orientation using a gradient descent algorithm. In *2011 IEEE International Conference on Rehabilitation Robotics*.

Marchese, A.D. and Rus, D. (2016). Design, kinematics, and control of a soft spatial fluidic elastomer manipulator. *The International Journal of Robotics Research*, 35(7), 840–869.

Rus, D. and Tolley, M.T. (2015). Design, fabrication and control of soft robots. *Nature*, 521(7553), 467.

Valtin, M., Salchow, C., Seel, T., Laidig, D., and Schauer, T. (2018). Modular finger and hand motion capturing system based on inertial and magnetic sensors. *Current Directions in Biomedical Engineering*, 3(1), 19–23.